

MESOSCALE WINDS IN VICINITY OF CONVECTION AND WINTER STORMS

Robert M. Rabin

NOAA/National Severe Storms Lab (NSSL), Norman, OK
Cooperative Institute for Meteorological Satellite Studies (CIMSS), Madison, WI

ABSTRACT

Winds obtained from tracking features in satellite imagery have been used primarily to improve analyses and forecasts over ocean areas. In order to explore the use of target-tracked winds in nowcasting convection over land, the CIMSS water vapor wind tracking algorithm is being applied to GOES-8 data on an experimental basis at 30-minute intervals in near real-time over much of the U.S. The amount of editing of wind vectors is reduced in order to include larger deviations from the model 'guess' fields. This allows the detection of perturbed flow aloft due to convection and other mesoscale features not correctly captured by models. Analyses from the wind fields include the display of wind vectors and objectively analyzed divergence, absolute and relative vorticity, and isotachs at 300 hPa. Comparisons are also available between the analysed fields of divergence, vorticity, and isotachs and those from global and mesoscale forecast models. The output of these products with interactive displays is available on the web (<http://zonda.ssec.wisc.edu/~rabin/real.html>). In addition, derived wind fields are available on N-AWIPS displays at the NOAA Storm Prediction Center (SPC) on an experimental basis.

The upper air wind fields from the algorithm are presented for a variety of convective and winter storm events. Winter storm cases usually reveal a consistent relation between divergence aloft and precipitation evolution, especially near convective cloud tops. Investigation of several convective systems indicate a lack of significant vorticity or divergence perturbations aloft before convective development. With areal growth of these systems, divergence and vorticity signatures emerge and occasionally persist after the demise of the active convection. Given the presence of divergence aloft on a scale of at least 200-300 km, the thunderstorm clusters usually persist for several hours over similar horizontal scales. In some cases with weak forcing, convective systems developed in the vicinity of upper ridges near a minimum in absolute vorticity (with values $< 4 \times 10^{-5} \text{ s}^{-1}$). These values were only slightly above the threshold for inertial stability, suggesting a possible role of this mechanism in MCS growth.

1. Introduction

Forecast applications of water vapor imagery have relied on the subjective interpretation of upper-level features from the imagery (Weldon, R.B., and S.J. Holmes, 1991) and comparison with their location and intensity in forecast models. Winds obtained from tracking features in the imagery have been used to improve analyses and forecasts over ocean areas. In order to explore the use of target-tracked winds in nowcasting over land, the water vapor wind tracking algorithm developed at CIMSS (Velden et al., 1997) has been applied to GOES-8 data on an experimental basis at 30-minute intervals in near real-time over much of the U.S. This is about 6 times more frequent than the operational water vapor wind products, which are produced at 3-hourly intervals. More importantly, the amount of wind vector editing has been greatly reduced in order to include larger deviations from the model 'guess' fields. This allows the detection of perturbed flow aloft due to convection and other mesoscale features not correctly captured by models.

This paper examines the upper level wind fields deduced from water vapor imagery for a variety of winter storms and summertime convective events. The analysis technique is briefly described in Section 2. Results are presented in Section 3. A summary is given in Section 4.

2. Method

The first wind tracking techniques required manual interaction with the computer to identify common cloud features in successive satellite images. Wind vectors were then estimated from the displacement of features and the time interval between images. The height of each wind vector was estimated from cloud top temperature (from the window channel radiance) and vertical soundings of temperature. More recently, the process has been automated and expanded to track features in water vapor imagery. The automated technique is described in Veldon et al. (1997). It consists of target identification, height assignment, wind calculation, and editing. The automated technique relies on a background wind field to facilitate the location of common features between successive images. The Navy Operational Global Atmospheric Prediction System (NOGAPS) model (Rosmond, 1992) is used as the background field. By employing a lower resolution model such as the NOGAPS, the addition of higher resolution winds from the satellite is more clearly identifiable. For most of the cases presented in this paper, the background wind field was updated only every 6 hours. Current implementation utilizes time interpolation to provide hourly updates of the background wind field between forecast output times. It is important to note that the winds from features tracked in water vapor imagery (other than clouds) are not associated with a single altitude. Rather, these winds are representative of layers, weighted in the vertical in accordance with the weighting function of the 6.7 micron GOES image channel. Typically, most of the weight comes from a layer 200-300 hPa deep. The altitude of the weighting functions varies directly with upper level moisture. Typically, mean layer heights vary from 400 hPa in dry areas to 200 hPa where upper level moisture is high. Wind vectors directly associated with thick high clouds, such as anvil tops, are from a single level near cloud top.

Since the mean height of wind vectors vary over a given region, it is necessary to interpolate the values to a constant altitude before evaluation of horizontal gradients required in the computation of kinematic parameters such as vorticity and divergence. For this purpose, an objective analysis is used which combines available wind vectors with the background wind field at constant pressure levels from the NOGAPS forecast model. Grid spacing of about 100 km has been used for the analysis. For purposes of this study, analyses centered near 300 hPa are used for evaluation of divergence, absolute and relative vorticity, and wind speed. This layer includes the anvil region of deep convection where upper level divergence can be strong and related to the mesoscale upward air motion. Because of the vertical weighting of the water vapor winds, the derived quantities such as divergence and vorticity represent vertical averages centered near 300 hPa. Caution should be observed in interpreting the kinematic properties near dry areas where no satellite winds may be available near 300 hPa. The objective analysis will be based mainly on the background wind field in such areas. A map of wind vectors should be examined to ensure adequate coverage in the layer 200-400 hPa.

3. Analyses

Analyses from the wind fields include the display of wind vectors and objectively analyzed divergence, absolute and relative vorticity, and isotachs at 300 hPa. The output of these products is available for real time data and for archived cases on the Web at <http://zonda.ssec.wisc.edu/~rabin/real.html>.

The web page includes interactive displays for animation of water vapor imagery and overlays of derived parameters. Comparisons are also available between the analyzed fields of divergence, vorticity, and isotachs and those from the NOGAPS and Rapid Update Cycle (RUC-2) model

(Benjamin et al., 1998). The following are a few examples of wind analyses typical of wintertime storms with widespread precipitation and for localized convective storms.

a. *Winter Storms*

On 26 January 2000, a widespread area of snow developed across central Oklahoma producing 10-15 cm of accumulation (~12-23 UTC). The snowfall appeared to be related to isentropic lift associated with warm air advection. This snow event was not well predicted. It occurred well downstream of an upper level trough, which moved across the region on 27 January. Snow had been forecasted (at least a couple of days in advance) to begin after 00 UTC on the 27th. The upper system produced convective precipitation further east on the 27th. Freezing rain and ice pellets effected north Texas & the heaviest snow fell in parts of eastern Oklahoma with as much as 17" reported in Eufaula, Oklahoma.

In general, the RUC-2 wind fields contain more structure than the satellite winds because of the model's high resolution. The RUC-2's upper level divergence field seems to match the location of the snow band on 26 January more consistently than the satellite analysis (Fig. 1). The satellite analysis developed a circular shaped divergent area over eastern Oklahoma by 17:45 UTC. Note that the analyzed divergence pattern is significantly different from the background field, which was nearly 6 hours old at the time of analysis. The RUC-2 indicated an elongated area of divergence just south of the reflectivity band starting by 15:45 UTC. The divergence visible from satellite may have been limited or distorted due to the shallow nature of the upward motion during the warm air advection phase of the storm.

A strong divergence couplet developed with the upper low as it tracked across Oklahoma by 15 UTC on 27 January (Fig. 2). The most intense divergence was located over the convective cloud region centered near the southeast tip of Oklahoma. Strong convergence was located to the west near the leading edge of a dry band aloft. The RUC-2 and the background NOGAPS fields indicate the divergence further west in western Oklahoma. Note that the background field was 3 hours old at the time of the analysis. Despite this, the satellite analysis captured the eastward movement and evolution of intensity.

Additional examples of winter storms are available on the web at <http://www.nssl.noaa.gov/~rabin/paper/windpaper.html>. These include two significant snowstorms in the upper Midwest on 11 and 18 December 2000, and a severe ice storm, which effected parts of Oklahoma and Arkansas on 25-26 December 2000. In these events, radar echoes were widespread through the area of divergence. In the first two cases, the highest radar reflectivities were south of the area with maximum divergence, although heaviest snowfall was in vicinity of the divergence. The high reflectivities to the south may have been due to mixed precipitation in these areas. In addition, displacement of the divergence pattern to the north due to a slope of upward air motion with height was a possible factor. In the case of the ice storm, strong divergence was observed in areas of convective precipitation.

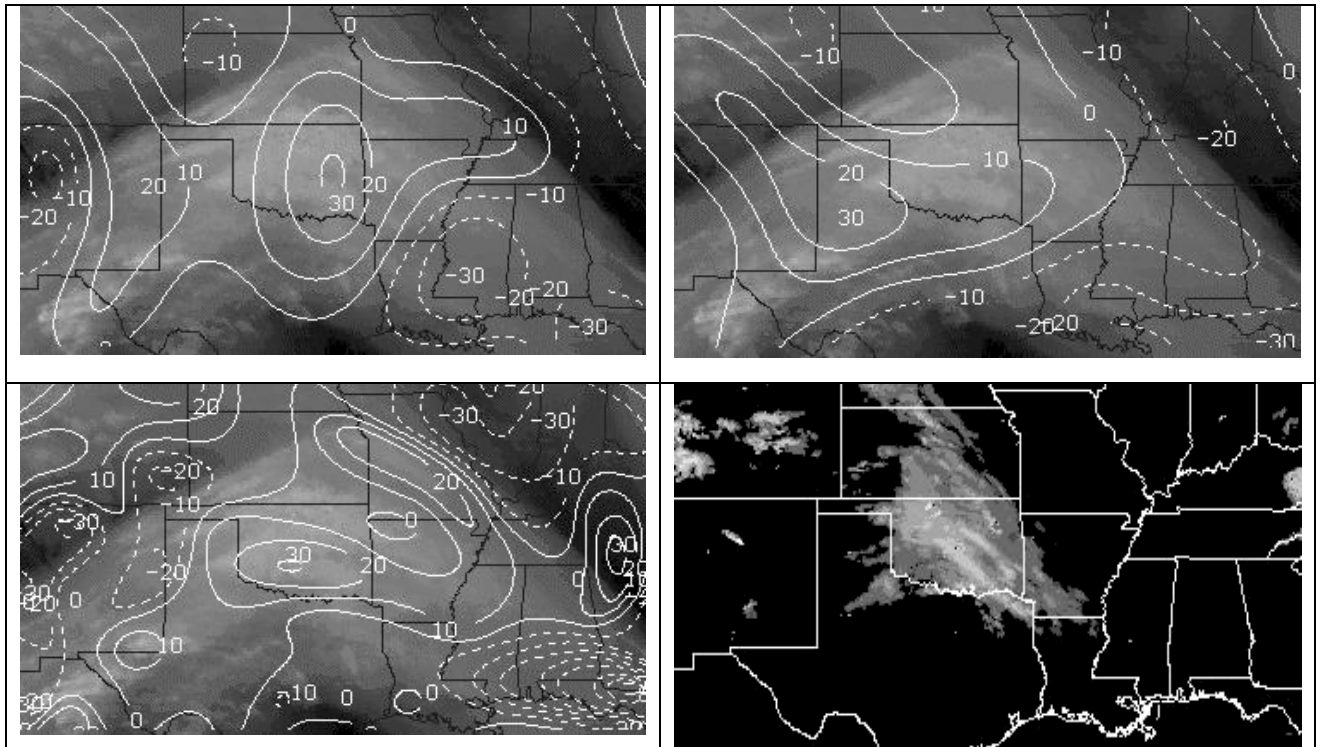


Figure 1. Water vapor image and divergence at 300 hPa ($10^{-5} s^{-1}$) at 1745 UTC, 26 January 2000 from water vapor winds (top left), background wind field (top right), RUC-2 (lower left). Radar reflectivity at the same time (lower right). Maximum reflectivity is about 30 dbZ.

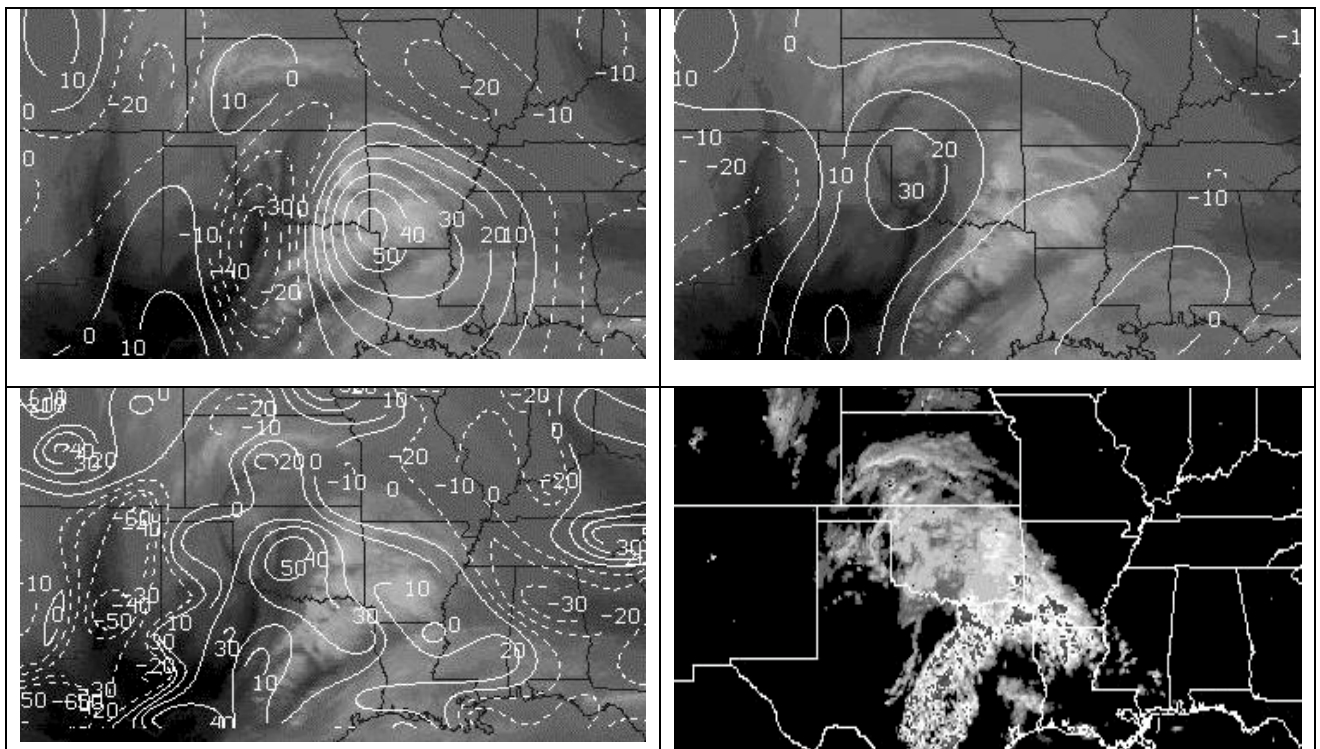


Figure 2. Water vapor image and divergence at 300 hPa ($10^{-5} s^{-1}$) at 1545 UTC, 27 January 2000 from water vapor winds (top left), background wind field (top right), RUC-2 (lower left). Radar reflectivity at the same time (lower right). Reflectivity exceeds 40 dbZ where dark shading repeats.

b. Warm Season Convection

An example of strong mesoscale forcing occurred in Oklahoma and Kansas on 3-4 May 1999. Multiple supercell thunderstorms produced over 70 tornadoes after 2100 UTC on 3 May. Figure 3 shows upper level wind fields at early (2145 UTC) and later (0045 UTC) stages of the convective outbreak. Of interest was the wind maximum near the Oklahoma and Texas panhandles about 500 km to the west-northwest of the convection at 2145 UTC. An upper level trough was centered to the west in New Mexico and Colorado. The trough and wind maximum had moved from south central Arizona and southwest New Mexico respectively at 1200 UTC. The convection formed on the anticyclonic side of the wind maximum near a minimum in relative vorticity ($-20 \times 10^{-6} \text{s}^{-1}$). Peaks in divergence developed over the convection and ahead of the main trough in eastern New Mexico, however the intensity was not unusually strong as compared to other convective events. By 4 May 0045 UTC, the wind maximum had shifted east and was near the western edge of the active convection. Also, the convection was centered between a couplet of cyclonic and anticyclonic vorticity. Comparisons of upper level fields were made with the operational ETA (Black, 1994) and RUC-2 models. The models did well in depicting the divergence above the convection and the vorticity couplet at 00 and 06 UTC on 04 May. Earlier, there are differences between the satellite, RUC-2 and ETA fields.

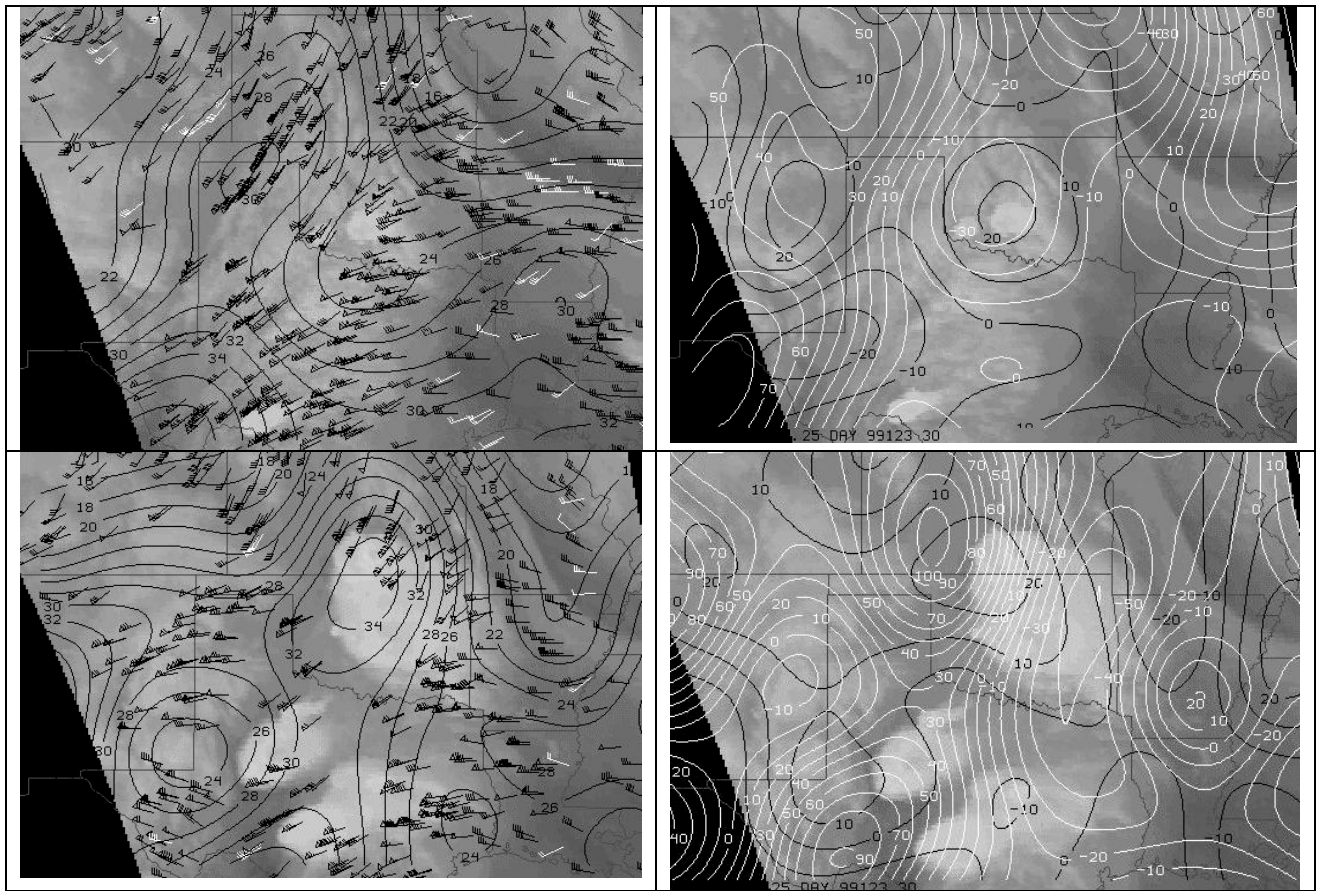


Figure 3. Left panels: Wind barbs (Thick black 100-250 hPa, thin black 250-350 hPa, white 350-500 hPa) and isotachs (m s^{-1}). Right panels: Relative vorticity (10^{-6}s^{-1}) in white, divergence (10^{-5}s^{-1}) in black, 03 May 1999, top row: 2145 UTC, bottom row: 04 May 1999, 00:45 UTC.

Mesoscale Convective Systems (MCS) often develop under weak upper forcing during the summer months in the U.S. Fueled by moisture and warm air advection in the low levels, they typically occur in vicinity of upper level ridges. Blanchard et al. (1998) proposed a role of inertial instability in the growth of MCSs by enhancement of upper level divergence. Using upper wind analyses from rawinsonde data, the occurrence of negative absolute vorticity, a necessary condition for inertial

instability, accompanied the onset of large systems. The absolute vorticity was examined here using the satellite wind analyses for events with weak forcing.

The time series of maximum divergence was examined for a large MCS lasting 14 hours on 20 July 1995, Figure 4 (left panel). This system was associated with a frontal boundary and had an elongated shape rather than the more circular pattern typical of Mesoscale Convective Complexes (MCC). In this case, the time trend of maximum divergence appears related to the evolution of the MCS as observed from the coverage of the cold cloud shield in the infrared satellite imagery, Figure 4 (right panel). The strongest divergence was near the end of the mature phase (2-5 UTC). There was a rapid decline after 0530 UTC, near the onset of decay. However, the decline in divergence did not continue during the decay phase (5-8 UTC) when values remained nearly constant at $60 \times 10^{-5} \text{ s}^{-1}$.

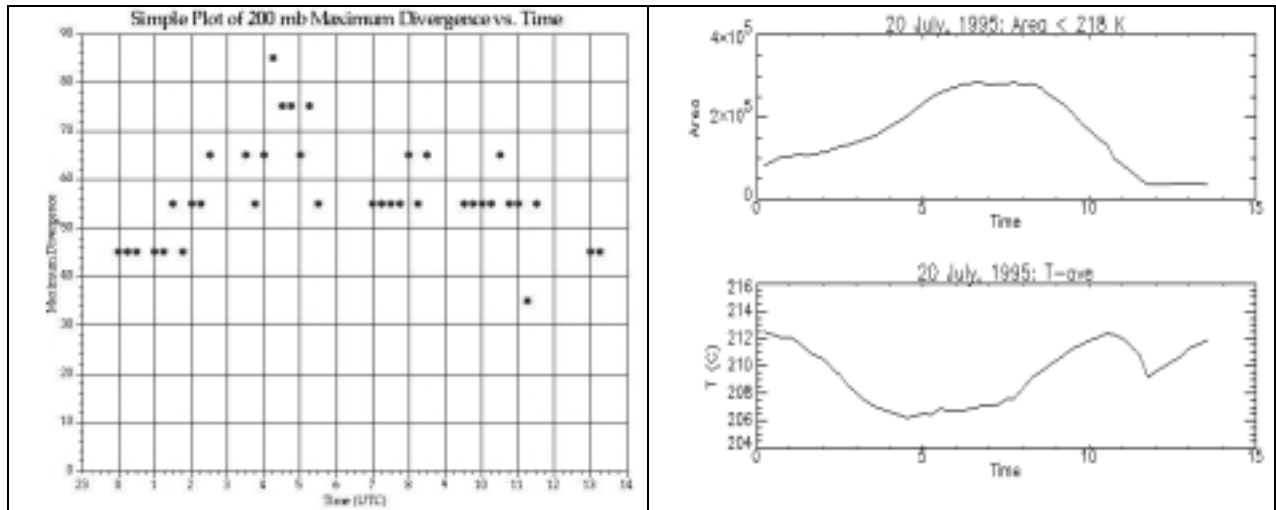


Figure 4. Left: Maximum divergence (10^{-5} s^{-1}) vs. time. Right, top: Area in km^2 of cloud top colder than -55°C , bottom: mean cloud top temperature ($^\circ \text{K}$) vs. time.

The spatial distribution of divergence and absolute vorticity at 15-minute intervals is available on the web site: <http://www.nssl.noaa.gov/wrd/cw/uswrp/winds.html>. During the early stages of development (23-03 UTC), the minimum absolute vorticity was just southeast of the convection. Perhaps this was a factor in the observed expansion of the cloud shield to the southeast. During the mature phase, the minimum absolute vorticity was aligned roughly with the convection, however the minimum was located downwind (northeast) from the most active area. In these areas, the absolute vorticity became negative. During the decay phase, the minimum remained aligned with the convective cloud, but was slightly positive.

Additional examples of wind fields near mesoscale convective systems are available on the web at <http://www.nssl.noaa.gov/~rabin/paper/windpaper.html>. A variety of systems are presented there. The major observations are summarized in Table 1. More than half of these cases formed near the axis of an upper level ridge. Systems formed or evolved near local minimum of absolute vorticity in approximately half the total number of cases. The absolute vorticity was observed to be negative in only one case. On several occasions, initiation and propagation occurred along a band of uniform gradient in absolute vorticity. These areas were near maximum speed shear to the anticyclonic side of a wind maximum. Often, the convection moved toward areas of lower absolute vorticity after weakening. In some cases, cirrus debris could be tracked long after dissipation of the active convection and regeneration occurred in areas of low absolute vorticity. The shorter-lived systems were generally accompanied by weak divergence aloft. In some cases, strong divergence was observed during intensification of these systems.

Table 1. Characteristics of additional convective systems and 300hPa wind features. Absolute vorticity is given in units of 10^{-5} s^{-1} .

Date	Size/Duration	Upper Flow	Absolute Vorticity	Divergence
15 July 2001	~ 16 h moderate size	Southwesterly West of ridge axis	Anticyclonic side of jet max 2 - 4	Strong
4 July 2000	~ 16 h 2 Clusters merged Intermittent intensity	Southwesterly/near ridge axis	Located in gradient 6 - 8	Weak Peak during merge and intensification
20 July 2000	~ 14 h reformation next afternoon	Zonal Formed just north of maximum speed shear	Initially in gradient, then near minimum 2 - 6	Locally strong couplet persisted for several hours
9 August 2000	~ 15 h Small cluster, associated with Derecho	West northwesterly fast flow	South of max gradient Near minimum 4 - 6	Weak
19 July 2000	~ 8 h Small cluster	West southwesterly near ridge axis	Formed near weak maximum 6-10	Variable
03 July 2000	~ 5 h propagated southeast Cirrus debris persisted for > 13 h	Top of high amplitude ridge Near right entrance region of wind max.	Negative during intensification Cirrus debris remained near minimum (0-2)	Strong divergence during onset
11 July 2000	~ 5 h propagated southeast	Near top of ridge No local wind maximum observed	Near minimum at onset (<4), 6 - 8 during dissipation	Weak
05 July 2000	~ 8 h formed near sunrise regeneration by late afternoon	Southwesterly flow Near northern edge of max speed shear	Initially near maximum gradient (4-8), Then to south (4 -6)	Weak

4. Summary and Conclusions

The CIMSS water vapor wind tracking algorithm has been implemented to allow the detection of perturbed flow aloft due to convection and other mesoscale features. The horizontal resolution of wind fields is limited by the density of targets, tracked by the automated technique, and the resolution of the objective analysis. For example, the fields of divergence and vorticity do not contain as much detail as RUC-2 analyses.

Examination of winter storm cases reveals a consistent relation between divergence aloft and precipitation evolution, especially near convective cloud tops. In some cases, the divergence can be displaced downwind due to shear. Divergent areas may not be detectable from the water vapor wind analysis where air ascent is limited to shallow layers.

Investigation of several MCS's confirm the lack of significant vorticity or divergence perturbations aloft before convective development. With areal growth of these systems, divergence and vorticity signatures emerge and occasionally persist after the demise of the active convection. Given the presence of divergence aloft on a scale of at least 200-300 km, the thunderstorm clusters usually persist for several hours over similar horizontal scales. In contrast, isolated thunderstorms are often too small to be resolved by the satellite wind analysis and appear to develop in areas with no preferred sign of divergence. However, the rapid intensification of divergence is observed occasionally with the explosive growth of a single storm.

The absolute vorticity was examined using the satellite wind analyses for events with weak forcing. In many cases, convective systems developed in the vicinity of upper ridges near a minimum in absolute vorticity (with values $< 4 \times 10^{-5} \text{ s}^{-1}$). These values were only slightly above the threshold for

inertial stability, suggesting a possible role of this mechanism in MCS growth. However, it is important to note that inertial instability can be ruled out in other cases where absolute vorticity was relatively high.

Derived wind fields have been made available to the NOAA Storm Prediction Center (SPC) on an experimental basis. The operational value of these products in forecasting storm evolution remains to be determined. The principal limitations of the water vapor wind analysis are the variable nature of the target heights and the lack of vertical profiling. The future implementation of the Geostationary Imaging Fourier Transform Spectrometer (GIFTS) by NASA has the potential to provide analysis of water vapor winds at multiple levels.

5. Acknowledgments

We wish to thank Steve Wonzong, Tim Olander, David Stettner, and Chris Velden, of the CIMSS for their encouragement and assistance in setting up the software for satellite winds processing. Also, the concept of satellite winds would not have been possible without the foresight of Dr. Vern Suomi and early developers at the University of Wisconsin Space Science and Engineering Center from the 1970's onward.

REFERENCES

- Benjamin, S.G., J.M. Brown, K.J. Brundage, B.E. Schwartz, T.G. Smirnova, and T.L. Smith, 1998: The operational RUC-2. Preprints, 16th Conference on Weather Analysis and Forecasting, AMS, Phoenix, 249-252.
- Black, T.L., 1994: The new NMC mesoscale Eta model: Description and forecast examples. *Wea. Forecasting*, **9**, 265-278.
- Blanchard, D.O., W.R. Cotton, and J.M. Brown, 1998: Mesoscale circulation growth under conditions of weak inertial instability. *Mon. Wea. Rev.*, **126**, 118-140.
- Rosmond, T.E., 1992: The design and testing of the Navy Operational Global Atmospheric Prediction System. *Wea. Forecasting*, **7**, 262-272.
- Velden, C.S., C.M. Hayden, S. Nieman, W.P. Menzel, S. Wanzong and J. Goerss, 1997: Upper-tropospheric winds derived from geostationary satellite water vapor observations. *Bull. Amer. Meteor. Soc.*, **78**, 173-195.
- Weldon, R.B., and S.J. Holmes, 1991: Water vapor imagery: Interpretation and applications to weather analysis and forecasting. NOAA Tech. Rep. NESDIS 67, 213 pp.